J Mater Sci: Mater Electron (2017) 28:11059–11069
DOI 10.1007/s10854-017-6890-x

Effect of Ag clusters doping on the photoluminescence, photocatalysis and magnetic properties of ZnO nanorods prepared by facile microwave-assisted hydrothermal synthesis

R. P. A. Souza[1] · F. V. Motta[1] · J. H. O. Nascimento[2] · M. R. D. Bomio[1] · F. M. M. Borges[3] · M. A. Correa[4] · E. Longo[5] · M. S. Li[6] · F. Bohn[4] · C. A. Paskocimas[1]

Received: 31 January 2017 / Accepted: 30 March 2017 / Published online: 13 April 2017

Abstract We report a chemical route to synthesize stabilized ZnO:Ag nanoparticles (NPs) combined with nanosized metallic Ag using microwave-assisted hydrothermal synthesis. We employ X-ray diffraction (XRD), field emission guns scanning electron microscopy, transmission electron microscopy, spectrophotometry, photodegradation, photoluminescence and magnetic characterizations to investigate the structural, morphological, photocatalytic and magnetic properties of ZnO:Ag samples with different Ag concentrations. We verify through XRD results the standard wurtzite crystalline phases and face-centered cubic for metallic Ag NPs. Moreover, we confirm through spectrophotometry the photocatalysis in the samples. The Ag clusters doping the pure material causes the shift from green to yellow-red, which are lower energy wavelengths, thus corroborating changes of its electrical properties due to the decreased gap. We interpret the magnetic properties in terms of the nanosizing and similar effects. Under these conditions, we show the improvement of the photocatalytic and magnetic properties of ZnO NPs.

✉ R. P. A. Souza
renata.priscilla.souza@gmail.com

C. A. Paskocimas
paskocimas.ufrn@gmail.com

[1] Departamento de Engenharia de Materiais, Universidade Federal do Rio Grande do Norte, Natal, RN 59078-900, Brazil

[2] Departamento de Engenharia Têxtil, Universidade Federal do Rio Grande do Norte, Natal, RN 59078-900, Brazil

[3] Escola de Ciências e Tecnologia, Universidade Federal do Rio Grande do Norte, Natal, RN 59078-900, Brazil

[4] Departamento de Física, Universidade Federal do Rio Grande do Norte, Natal, RN 59078-900, Brazil

[5] Universidade Federal de São Carlos, São Carlos, SP 13565-905, Brazil

[6] Instituto de Física de São Carlos, Universidade Federal de São Paulo, São Carlos, SP 13566-590, Brazil

1 Introduction

Materials in nanometric dimensions may present unique properties arisen primarily due to the high surface/volume ratio. In this case, there is the increase of the number of atoms located on the surface of the nanoparticle, when compared to the number of atoms that are located in its inner region. Thus, many physical and chemical properties of nanostructured materials, for instance the short-range order and disorder level, emerge from defects present on the surface, such as electron/hole and oxygen vacancies.

Different techniques may be used to the obtainment of nanoparticles (NPs) from precursors. In particular, in literature, one can find methods including hydrothermal [1, 2], microwave-assisted hydrothermal [3, 4], precipitation [5], microemulsion [6], sol-gel methods [7], liquid combustion reaction [8], forced hydrolysis [9], spray drying [10], and Pechini method [11].

Among the several nanoparticulate materials, the semiconductor ones show some peculiar and interesting properties. Remarkably, the interpretation and elucidation of them have led to discoveries in different fields of science and technology [12]. Specifically, ZnO NPs have recently received great attention due to a variety of potential applications, such as UV absorption, deodorization and antibacterial treatment [13]. This semiconductor in the wurtzite structure (lattice parameters of a = 3.250 Å and c = 5.207 Å) has a direct band gap of 3.37 eV (368 nm) at room temperature, and it corresponds to one of the most

important inorganic materials with catalytic [14], electric [15, 16], optoelectronic [17, 18] and photochemical properties [19], which has increasingly stimulated extensive research on its applicability. On the other hand, Ag NPs can also act as a catalyst during a photocatalytic reaction. Some of the oxidative photocatalytic reactions are carried out with simultaneous reduction of Ag ions during deposition on the surface [20]. Thus, the photocatalytic properties of ZnO can be improved by engineering a composite consisting of ZnO:Ag, a material with higher electron transfer rate [21].

The photodegradation is one of the most effective route for degradation of organic pollutions to harmless materials, such as CO_2 and H_2O or other species in wastewater. One of the main obstacles for industrial applications of photocatalyst is the worry of the release and destiny of the photocatalysis in the environment. Therefore, it is favorable to recover and retain the catalysts. In this sense, NPs with a magnetic core are good candidates to overcome this problem [22].

Pure ZnO nanostructures are usually n-type and present weak optical features, that are caused by defects, such as oxygen vacancy or interstitial Zn; therefore they cannot be directly used in the industry. As a result, ZnO doping with a suitable element corresponds to an alternative for tailoring optical and magnetic properties. Although it is relatively difficult that ZnO achieves p-type doping, a limitation considered as an obstacle to the use of ZnO, elements of the groups 15, 1, and 11 have been identified to make possible this kind of doping. Moreover, transition metals or rare earth elements doping the ZnO have bring interesting results. In this sense, Ag is one of the best candidates due to its high solubility, high ionic size and low orbital energy [23].

The obtained diluted magnetic semiconductor has attracted considerable attention for prospective applications in multifunctional devices combining both, semiconductor and ferromagnetic functionalities. In particular, doping with a metal such as Ag, which has antibacterial properties, may enhance the antibacterial activity of the ZnO NPs, as well as improve other properties of interest. Thus, large efforts have been devoted to investigate ZnO:Ag compounds. However, the studies have been limited to synthesized particles with large sizes [24].

To explore the photocatalytic, antibacterial, and magnetic properties, the development of a technique to synthesize samples and control the growth of crystals becomes essential. Among the several techniques reported in literature to the obtainment ZnO:Ag, the hydrothermal method appears as a promising candidate to the production at low temperature of several crystalline metals and homogeneous high-purity oxides, with well-defined submicrometric and nanometric forms. However, regarding the versatility of the hydrothermal method, a peculiar feature related to its performance resides in the crystallization kinetics, which has low speed when the processing temperatures are above the supercritical one (≥374 °C), conditions which are desired for *Soft Chemistry Processes*.

In order to increase the crystallization kinetics, one may combine microwave energy to the hydrothermal process, thereby generating the microwave-assisted hydrothermal process. Currently, the synthesis of semiconductor oxides under microwave-assisted hydrothermal conditions constitutes an important aspect of materials processing due to their advantages in the preparation of high-quality nanomaterials with controlled size and shape for potential technological applications. In particular, there are many reports in literature regarding the preparation through microwave-assisted hydrothermal of various metal oxides, as TiO_2 [25], ZnO [23], CeO_2 [26], ZrO_2 [27], CuO [28], Al_2O_3 [29], Dy_2O_3 [30], In_2O_3 [31], Co_3O_4 [32], and NiO [33].

Here, we report a chemical route to synthesize stabilized ZnO:Ag NPs with nanosized metallic Ag using microwave-assisted hydrothermal synthesis. We investigate the structural, morphological, photocatalytic and magnetic properties of ZnO:Ag samples with different Ag concentrations. These results make this material commercially viable, due to the reduced need of operational energy to photodegradation of microorganisms, pollutants, soils, among others, as well as place the chemical route using microwave energy as a promising tool to produce stabilized NPs.

2 Experiment

For the study, samples of ZnO:Ag with different Ag concentrations are produced through a chemical route using microwave energy, and the structural, morphological, photocatalytic and magnetic properties are investigated.

2.1 Synthesis of the nanoparticles

Colloidal suspensions are prepared from metallic precursors of zinc acetate and silver nitrate, the latter as dopant at concentrations of 0, 1 and 2 mol% of silver ($ZnO_{x-1}Ag_x$).

The first step consists in to dissolve the two components in water with the aid of a magnetic stirrer. Thus, the solution pH is kept neutral, pH ≈ 7, while the water provides the hydrolysis of the zinc salt dihydrate ($Zn(OOCCH_3)_2 \cdot 2H_2O$, Alfa Aesar) and of the silver nitrate ($AgNO_3$, with 99.9% purity, Strem Chemicals).

After preparation, polyvinylpyrrolidone ($(C_6H_9NO)_n$, PVP, Alfa Aesar) is added to the solution as surfactant under magnetic stirring at 60 °C. After some minutes at the same temperature, hexamethylenetetramine ($C_6H_{12}N_4$, HTMA, Alfa Aesar) is added as a reducing/precipitation

agent. The final solution is reheated during 10 or 30 min using microwave energy at 100 °C. The chemical route is partly omitted here for future patent registration.

Similarly to any redox reaction, the values of the standard reduction potentials E^0 determine the pairs of reactants required to successfully chemical conversion. This means that the change of the free energy in the reaction must be negative, $\Delta G^0 < 0$, or equivalent, $\Delta E^0 > 0$. In the case of Ag, the electropositive reduction potential of $Ag^+ \rightarrow Ag^0$ in water is relatively large, $E^0 = +0.799$ V [34]. Equations (1), (2) and (3) are respectively synthesized, illustrating the precipitation chemical reactions involved in the synthesis of ZnO with HTMA.

$$(CH_2)_6N_4 + 6H_2O \leftrightarrow 6HCHO + 4NH_3, \quad (1)$$

$$NH_3 + H_2O \leftrightarrow NH_4^+ + OH^-, \quad (2)$$

$$2OH^- + Zn_2^+ \rightarrow ZnO(s) + H_2O, \quad (3)$$

Table 1 shows a summary of the colloidal suspensions aged by hydrothermal process under controlled chemical, temperature and time conditions. Samples are named according to the following order: host crystal (e.g., ZnO), synthesis time (e.g., 10 min) and the added Ag content (mol% Ag). They are produced using a steel autoclave with internal polytetrafluoroethylene container. Following, this autoclave is closed and heated by microwave, thus providing energy to the system and inducing the growth of the crystals. Here, a domestic Electrolux microwave Model MEF41 with frequency of 2.45 GHz is employed.

After all, the solution is centrifuged using a Centrifuge 5804 Eppendorf equipment. The obtained solid is taken to oven for 24 h at 85 °C. The resulting material is characterized and then photocatalytic reactions are carried out with doped and undoped material.

2.2 Characterization of the nanoparticles

The produced samples are characterized by X-ray diffraction (XRD) experiments, field emission gun scanning electron microscopy (SEM/FEG), UV–Vis spectrophotometry by absorbance and transmittance, photoluminescence (PL), as well as the magnetic response is verified.

Table 1 Solutions heated at 100 °C via microwave-assisted hydrothermal method to produce ZnO:Ag nanoparticles

Sample	Ag (mol%)	Microwave heating time (min)
ZnO10min-0	0	10
ZnO10min-1	1	10
ZnO10min-2	2	10
ZnO30min-0	0	30
ZnO30min-1	1	30
ZnO30min-2	2	30

2.2.1 X-ray diffraction

X-ray diffraction results are obtained with a Shimadzu XRD-7000 equipment with CuKα radiation ($\lambda = 1.5418$ Å), voltage of 40 kV and current of 40 mA. From the patterns, the crystallite size is calculated through the Scherrer's equation [23], with $k = 0.9$, λ as the wavelength, θ as the diffraction angle and B as the width at the half-height of the peak.

2.2.2 Photocatalytic properties

The photocatalytic activity is evaluated for all samples at concentration of 1 ppm. For this, a photoreactor with UV radiation emission with five Philips bulbs of 15 W and methyl orange dye at concentration of 10^{-5} mol/L is employed. Thus, the visible UV spectroscopy technique is used in samples collected every 30 min, with total time of 150 min. From this technique, it is possible to analyse the transmission, absorption and reflection of the material as a function of light wavelength. Electronic transitions are investigated in the region from UV to near infrared (200–800 nm). The measurements are performed with a Shimadzu UV-2600 spectrophotometer. Thus, we are able to obtain spectra in absorption modes and investigate the photocatalytic efficiency and the discoloration reaction kinetics of ZnO/(ZnO:Ag)+Ag^0 samples under orange methyl dye, which has approximate wavelength of 460 nm and is the reference wavelength for the study, as a function of radiation time.

2.2.3 Photoluminescence

Considering the photoluminescence technique, it is possible to obtain further information on the material and verify photoluminescent properties such as energy gap *Ebg*, being of direct or indirect source, identification of elements composing the sample, type of defects and impurities. For the photoluminescence measurements, a Jobin-Yvon U1000 spectrophotometer with double monochromator, cooled GaAs photomultiplier and a conventional photon counting system, is used. PL measurements are performed at excitation wavelength of 350.7 nm. Thus, the *Ebg* is given by

$$Ebg = \frac{hc}{\lambda}, \quad (4)$$

where λ is the wavelength in nanometers, $c = 3 \times 10^8$ m/s is the speed of light in vacuum, and $h = 4.135 \times 10^{-15}$ eV s is the Planck constant.

2.2.4 Magnetic characterization

The magnetic characterization is obtained by using a Quantum Design Dynacool Physical Property Measurement System. In this case, isothermal magnetization curves at 5, 10, 25, 50, 100, 300 and 500 K are obtained. Moreover, the temperature dependence of field-cooled (FC) and zero-field-cooled (ZFC) magnetization curves, acquired in the range of temperature between 5 and 300 K and under a constant field of 200 Oe, is investigated.

3 Results and discussion

3.1 Characterization of partial replacement (doping)

Figure 1 presents the XRD patterns for the ZnO:Ag samples with different Ag concentrations, synthesized with distinct microwave heating times. All the investigated samples have standard wurtzite crystalline phase (stable phase) for the ZnO (PDF NO. 36-1451, lattice parameter of $a = 3.2498$ Å and $c = 5.2066$ Å). The doped compositions present face-centered cubic structure for the metallic Ag NPs (PDF NO. 65-2871). Moreover, low-intensity hexagonal Ag peaks are also observed (PDF NO. 87-598) and, for the sample doped with 2% Ag at 10 min, the presence of hexagonal silver oxide (PDF NO. 42-874) is verified. Data from the lattice parameters are calculated using the Unit-Cell software.

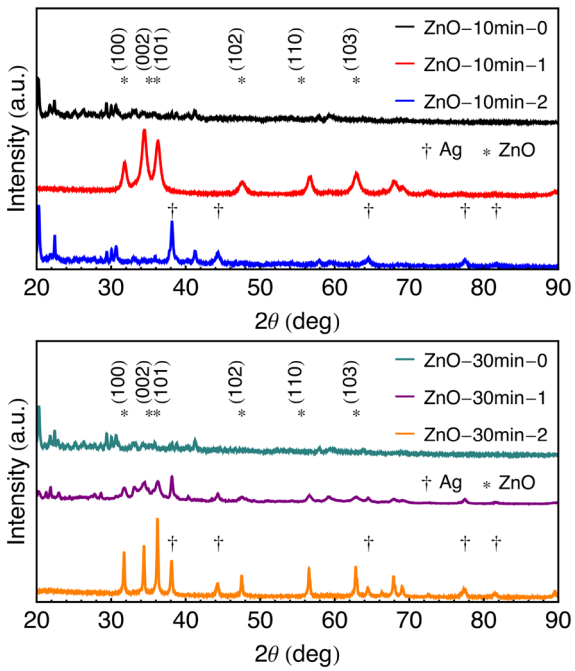

Fig. 1 X-ray diffraction for the for ZnO:Ag samples with 0, 1, and 2 mol% Ag and synthesis during 10 and 30 min

According to Ha et al. [35], the width of the half-height of the diffraction peaks grows rapidly with the increase of PVP concentration as surfactant, a fact associated with the reduction of the particle size. In particular, here, the PVP content is not changed for the different compositions. However, we observe that the Ag content and synthesis time influence the crystallinity of the material.

From Fig. 1, the diffraction peaks are related to the ZnO in the wurtzite phase and to the metallic Ag phase. Remarkable differences are verified in the diffraction patterns acquired for the pure material and the doped ones. For the ZnO10min-1 sample, the CFC Ag peaks are not observed, despite the addition of 1% Ag molecular weight during the synthesis. On the other hand, the ZnO30min-2 sample presents high-intensity peaks associated to the metallic Ag. A raise in the crystallinity of the wurtzite phase is also noticed, since there is an increase of the intensity and a decrease in the width at half-height of the ZnO (002) peak. These features indicate the partial substitution of the Ag in the ZnO structure (this fact is also confirmed through the PL results).

For the other doped compositions, the Ag peaks, attributed to the metallic phase, are also verified. Besides, an increase in the intensity of Ag peaks with the raise of the concentration and synthesis time is found. Regarding the wurtzite diffraction peaks, lower crystallinity is observed for the ZnO10min-0, ZnO10min-2 and ZnO30min-0 samples. In some cases, the reduction in the degree of crystallinity is evidenced in the XRD through the decrease of the intensity and increase of the width at half-height of the diffraction peaks, a fact that can also be observed in crystallites smaller than 1 µm. In the case of crystalline NPs, they share similar features for X-ray diffraction patterns, characterized by low-intensity and broad peaks [36]. It should be noted that the positions of peaks, mainly with respect to the Ag (100) plane, are displaced with the presence of Ag in the samples, as evidenced in Table 2. This shift suggests that there is partial substitution of Ag in the ZnO structure, as well as an increase or decrease of a and c lattice parameters, as expected. When an increase occurs, this result is presumably related with the difference in size of the Ag^{+} (0.115 nm) and Zn^{2+} (0.074 nm) ions. Some studies have shown slight reduction of these parameters, which can be explained by the formation of Ag clusters (Ag_{cl}) [23]. Notice that the a values, shown in Table 2, are smaller than the ones found to the ZnO bulk.

The XRD pattern suggests a trend to the orientation in the (101) plane, perpendicular to c-axis of the hexagonal ZnO network, which confirms that the structure corresponds to wurtzite. A reduction in the parameter a and increase in c are also observed, suggesting the production

Table 2 Solutions heated at 100 °C via microwave-assisted hydrothermal method to produce ZnO:Ag nanoparticles

Sample	2θ (°)	*hkl*	*a* (Å)	*c* (Å)	*D* (nm)
ZnO10min-0	31.78	(100)	2.8481	5.3908	13.59
ZnO10min-1	31.77	(100)	2.8512	5.4091	22.20
ZnO10min-2	31.85	(100)	2.8516	5.4090	15.97
ZnO30min-0	31.92	(100)	2.8400	5.4141	22.20
ZnO30min-1	31.85	(100)	2.8462	5.7545	21.16
ZnO30min-2	31.77	(100)	2.8498	5.3898	35.01

of nanorods. Extreme sharp ZnO nanorods result in a strong increase in an electric field. Therefore, they can be used as field emitters.

Figure 2 presents SEM/FEG images obtained for the produced samples. Residual polymer is observed after the synthesis in all samples. The morphology of all samples reveals a tendency to aggregation of the particles, which leads to the formation of porous agglomerates structures with irregular morphology. It is observed that the samples consist of smaller agglomerates adsorbed into larger agglomerates. This tendency to the agglomeration state occurs due to the attraction between the nanostructured particles (also identified through XRD and PL results), which constitute these clusters.

The formation of aggregates occurs due to very fine particles, particularly nanostructured particles with large specific area that frequently agglomerate to form secondary particles. This new conformation minimizes the total or interfacial surface energy of the system, and increases the stability [37]. The phenomenon of aggregation can be attributed to the growth and coalescence of nuclei, leading to the aggregation of the resulting particles, i.e. decreasing the specific area towards a lower energy state through the reduction of interfaces with the medium [34]. This is due to the low working temperature applied with the employed method, which results in the formation of extremely small crystallites (or particles) [38]. Here, when the particles are present in single crystals, the term crystallite can be used with the same meaning [39].

Bright spots are related to the Ag content. In particular, the higher the Ag concentration and synthesis time, more Ag NPs can be identified. Even in nanometric dimension, the particles can be visualized due to the intense brightness of the Ag. At the beginning of the precipitation, many small crystallites are formed (nucleation), but they tend to rapidly aggregate (growth) in order to form larger and thermodynamically stable particles.

Figure 3 presents electron transmission images for the pure ZnO sample and for the ZnO doped with 1 mol% of Ag, both for the 10 min synthesis. For the pure material,

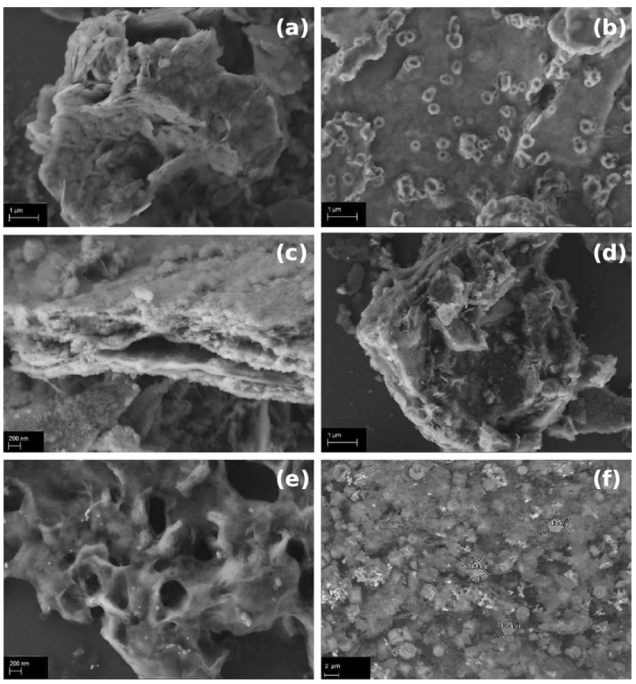

Fig. 2 In the *left*, SEM/FEG images of the ZnO:Ag samples synthesized at 10 min, with **a** 0, **c** 1, and **e** 2% Ag, respectively. In the *right*, images of the ZnO:Ag samples synthesized at 30 min with **b** 0, **d** 1, and **f** 2% Ag, respectively. The image size in **a**, **b**, **d** is 11 × 7.5 µm, in **c**, **e** the size is 5.3 × 3.6 µm, and in **f**, 45 × 31 µm

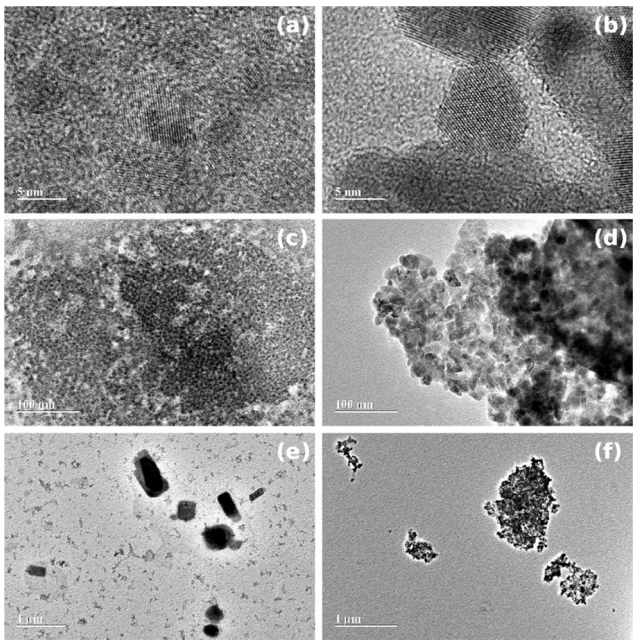

Fig. 3 In the *left*, **a**, **c**, **e** electron transmission microscopy images for the pure ZnO sample. In the *right*, **b**, **d**, **f** images for the ZnO:Ag samples doped with 1 mol% of Ag, both for the 10 min synthesis. The image size in **a**, **b** is 6.3 × 4.2 µm, in **c**, **d** the size is 630 × 420 nm, and in **f** 30 × 21 nm

the images confirm the presence of agglomerated ZnO NPs with average crystallite diameter between 5 and 10 nm.

The agglomerated powders use to retain the properties of the nanoparticulate units. However, in same cases, they lose the properties of the discrete units and resemble to highly defective bulk crystals. Whether the former or the latter is the case greatly depends on the property in question; thus, for example, whereas only mild agglomeration of magnetic and luminescent NPs, which would have comprised a superparamagnetic material if sufficiently separated, leads to appearance of unintended ferro- or ferri-magnetism [40].

For the doped material, it can be observed an agglomerated heterostructure of nanoparticulate hexagonal ZnO, with average crystallite diameter around 20 nm, decorated with Ag NPs. Moreover, the partial substitution of the Ag in the ZnO structure favors the growth of nanocrystals. These results are confirmed by XRD, SEM and photoluminescence.

The spectroscopic analyses in the UV–Visible region (UV–Vis) are obtained considering powders with and without dopants, synthesized at the same temperature with different synthesis times. All measurements are performed in the environment measurement. The gap is obtained by extrapolating the linear region of the curve according to the Tauc method, which relates the absorption curve and the energy gap of the material through

$$h\nu\alpha = A\left(h\nu - E^{opt}\right), \tag{5}$$

where α is the absorbance, h is the Planck constant, ν is the frequency, A is a proportionality constant and E^{opt} the optical gap of the band (Tauc gap). The value of the exponent denotes the nature of the electronic transition, indicating whether it is allowed or forbidden and whether it is direct or indirect. The absorption process arises when the light crosses the sample. The absorbed light is given by the difference between the intensities of incident I_0 and transmitted I radiations. The transmitted light may be expressed in term of both, transmittance and absorbance. The transmittance is defined as $T = I/I_0$. Absorbance α is related with the transmittance through $\alpha = \log(1/T) = -\log(T)$. The gap is obtained by extrapolating the linear region of the curve, according to the Tauc method. In insulator and semiconductor materials, there is an energy gap between occupied electronic states of lower energy and the unoccupied ones of higher energy. In particular, the magnitude of the energy gap distinguishes insulators and semiconductors. In a typical semiconductor, as Si, the energy gap is ~ 1.1 eV, while in an insulator, the energy gap is in the range between 5 and 10 eV. Thus, the gap is a critical parameter, determining the absorbed or emitted energy of the system.

In this context, the diffuse reflectance technique in UV–Vis is used as a tool to estimate the direct and indirect band gap values for the ZnO:Ag samples with different Ag concentrations. The range of wavelengths in the visible spectrum is between 400 and 700 nm, corresponding to photons with energy from 1.7 up to 3.1 eV. Thus, given that the direct optical gap of the ZnO is 3.37 eV, theoretically, the photons with energy in the visible range are able to cross the semiconductor without being absorbed, thus promoting high optical transmittance.

The doping of the ZnO with Ag promotes the substitution of a Zn atom (12B) by an Ag atom (11B). This replacement gives rise to imperfections that may create a sublevel formed by gaps above the valence band that, under these conditions, provide features of a p-type extrinsic semiconductor to the ZnO. Thus, the indirect gap can be accomplished by the excitation of an electron from the valence band to this sublevel and/or from this sublevel to the conduction band. The experimental curves obtained here for the indirect gap are consistent with this theory and are presented in Fig. 4.

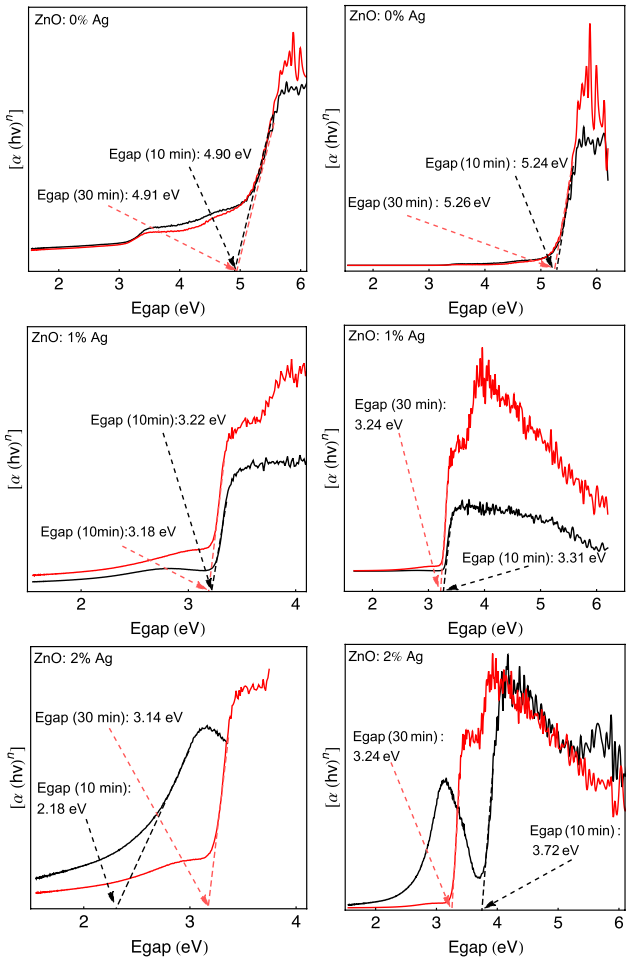

Fig. 4 Indirect (*left*) and direct (*right*) energy gap for the ZnO:Ag samples with 0, 1, and 2 mol% Ag and synthesis during 10 and 30 min

The theory proposed by Sugano–Tanabe describes the orbital division of the energy levels of transition metals such as Ag. In this case, the division is defined by the crystal symmetry. ZnO has a hexagonal anisotropic symmetry point group, as shown in Fig. 5. The load balancing reaction to the introduction of the Ag in the ZnO network can also be written as:

$$V_{Zn}^{2+} = 2Ag^{+}, \quad (6)$$

assuming that Ag^{+} substitutes Zn^{2+} in the tetragonal surrounding structure of the ZnO. Equation (6) shows that essentially two Ag^{+} ions are necessary to the compensation of Zn^{2+} loads. This provides a mechanism for the nucleation of Ag NPs in the ZnO host, such as Ag dimers [41], giving rise to considerable changes of the direct energy gap of the ZnO in the doped compositions.

The indirect energy gap appears for precursor materials with imperfections and, consequently, affects the intermediate energy level between the bands [42]. The quantum confinement of electron–hole pairs (excitons) leads to an increase in energy gap between the valence and conduction bands (direct band gap) of the material as the particle size decreases [43]. For the pure ZnO samples, the degree of perfection is high and the indirect gap assessment is not necessary (calculated for registration). Relating this fact to Figs. 1 and 2, XRD and FEG, NPs with high degree of crystallinity are obtained in pure and doped samples, a fact verified through the XRD and FEG results previously shown in Figs. 1 and 2, and it may explain the increase of the gap in the pure ZnO, synthesized during 10 and 30 min, and in the ZnO doped with 2% Ag synthesized during 10 min.

3.2 Heterogeneous photocatalytic degradation

Figure 6 presents the photocatalytic tests, performed under UV radiation, obtained for the produced samples. The most interesting result resides in the response of the

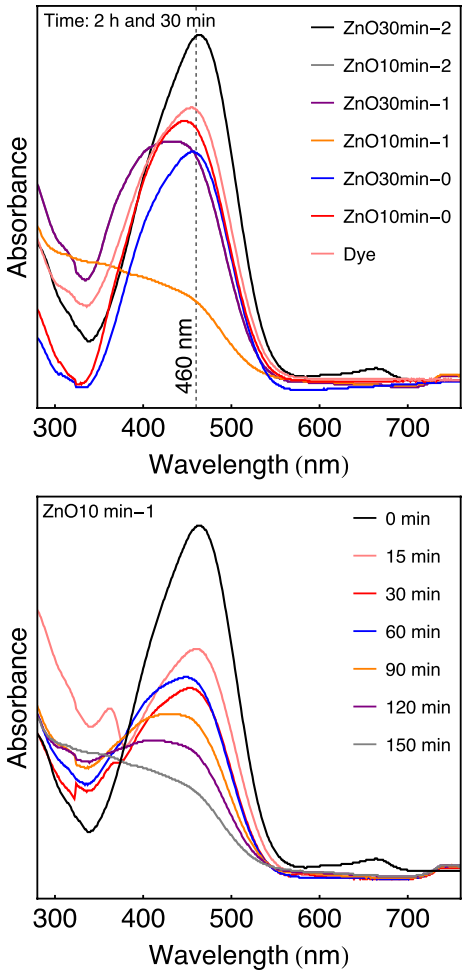

Fig. 6 Above, the absorbance spectrum for the produced samples as a function of the wavelength of methyl orange degradation measured in the photocatalytic reaction. Each photocatalytic test is performed during 2 h and 30 min. Below, the absorbance spectrum for the ZnO10min-1 as a function of the wavelength of methyl orange degradation at every 30 min

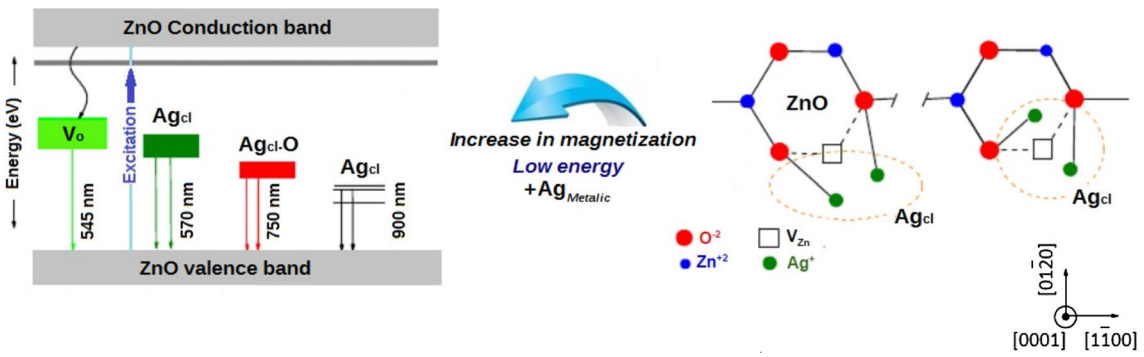

Fig. 5 Representation of the effect on the ZnO of the partial substitution of Zn by Ag_{cl}. In the *left*, schematic diagram for the excitation and emission for pure and doped ZnO. In the *right*, two possible configurations representing the substitution of a Zn^{2+} vacancy by an Ag dimer [41]

ZnO30min-2 sample. In this case, satisfactory photocatalysis is verified at the fixed time of 2 h and 30 min, presenting the highest absorbance value in the wavelength of the reference dye, when compared with the responses of the other compositions.

It is also observed that the ZnO samples without dopant do not effectively perform the photocatalytic process and also show broad Tauc gap. This gap condition may not favor the photocatalytic reaction, since the electrons in the valence band must jump to the conduction band. Another possibility which prevents the material from being a photocatalyst resides when electrons in the valence band jump very slowly to the conduction band.

The other samples perform insufficiently photocatalytic process, with indirect gaps smaller than 3.22 eV. However, the samples with dopant may not have shown a slow process of recombination, despite the high specific area, low-intensity photoluminescence and lower energy gap. Therefore, the ZnO10min-1 sample, which has no XRD peak associated with the metallic Ag NPs, is chemically inert, stable in the applied conditions, and of easy production and use, being thus a semiconductor to be applied as a photocatalyst.

The performance of a photocatalyst in a degradation process depends on factors such as the photocatalyst itself, concentration, its form of being present in the reaction, and doping. Some features deemed advantages of photocatalysis are: high specificity, uniform particle size distribution, spherical particle shape and the absence of internal porosity [44].

Figure 7 shows the photocatalytic activity C/C_0 as a function UV exposure time for the ZnO10min-1 sample. In this case, it is assumed a pseudo first-order reaction and C is the dye absorbance at 460 nm. We observe that the ZnO10-1 sample at 150 min of UV irradiation degrades 75% of the initial dye concentration. The degradation rate is given by $\ln(C_0/C) = k_{ap}t$, where k_{ap} is the the apparent velocity constant. Thus, by considering the plot of $\ln(C_0/C)$ as a function of the time, shown in the inset, we confirm a linear dependence, whose slope of the straight line corresponds to the value of the apparent velocity constant. The discoloration constant value k_{ap} of the degradation reaction is 0.0079 min^{-1}, a value compatible with the ones found in literature [45], and the correlation coefficient is $R = 0.9343$, with $R^2 = 0.87$.

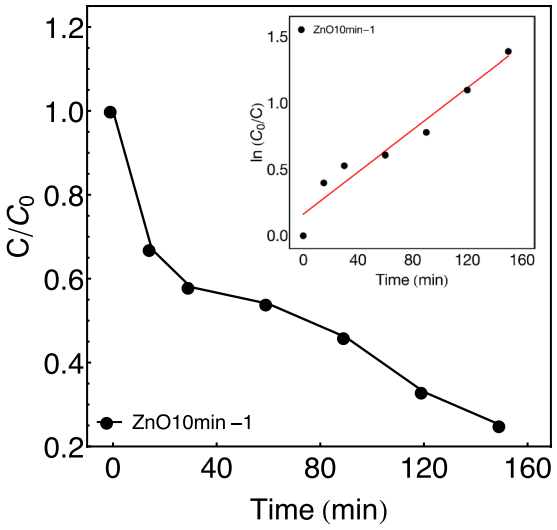

Fig. 7 Photocatalytic activity C/C_0 as a function of UV exposure time (0, 15 (ultrasound), 30, 60, 90, 120 and 150 min) for the ZnO10min-1 sample. The inset shows the linear regression of $\ln(C_0/C)$ also as a function UV exposure time

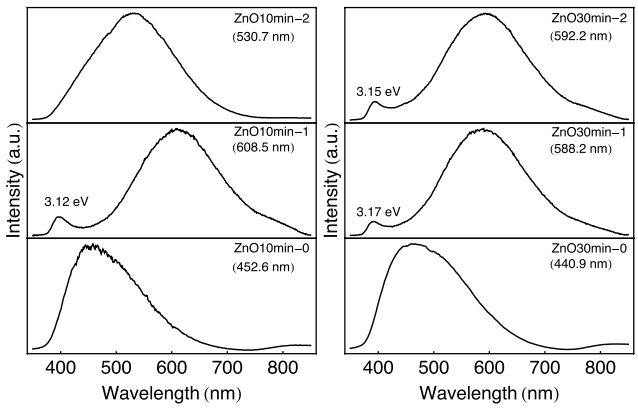

Fig. 8 In the *left*, photoluminescence results for the ZnO:Ag samples with 0, 1, and 2 mol% Ag and synthesis during 10 min. In the *right*, similar plot for the samples with synthesis during 30 min

3.2.1 Photoluminescence

Photoluminescence is the emission of electromagnetic radiation (photons) of a material after being submitted to light excitation. The frequency of the photon emitted by the sample is closely related to the type of material, since it is the result of an electronic transition. Each peak in the spectrum indicates a well-defined energy transition of excitations. Photoluminescence has also been extensively used to investigate defects in ZnO, such as the ones caused by ion implantation (partial substitution), and even as an indicator of the crystal growth rate during the production. The half bandwidth (peak width at half-height) is directly related to the crystal purity and as narrower the peaks, less the number of impurities (dopants) in the analysed crystal.

Figure 8 shows the PL spectra for the produced samples. Notice that the spectra exhibit remarkable differences for each sample, suggesting that changes in the emissions are caused by defects arisen from the doping with Ag and the heat treatment. The main features of PL spectra obtained at

low intensity can be divided into two categories, according to the observed peaks: narrow peaks for undoped samples; peaks close to the UV emission of about 390 nm (for some of the doped samples) and with a broad visible emission for all the samples doped with Ag. The low intensity found in all peaks is closely related to the crystallinity degree of samples found in the XRD. All ZnO/(ZnO:Ag)+Ag^0 NPs samples show high crystallinity, justifying the low emission intensity peak by PL.

The pure ZnO material in the wurtzite phase, prepared by the microwave-assisted hydrothermal method, may present nanocrystals that are not stoichiometric. In this case, they have usually an excess of Zn atoms and oxygen vacancies, which are indicators of many lattice and superficial defects in the crystals. These defects act as non-radiative centers and reduce light emission. Blue and blue-green emissions are possibly due to surface defects in the ZnO NPs, and the low intensity of the green emission may be associated to the smaller density of oxygen vacancies (2.69–2.74 eV) [46].

From the absorption spectra in the UV–Visible (2.34–2.04 eV) of the ZnO:Ag samples with different Ag concentrations, one can find a peak around 390 nm that emerges with the increase of the Ag content. This band is verified with red shift (up to 608.5 nm), which expands and increases in intensity as the amount of Ag partially substituted in the host ZnO is raised [47]. The yellow defect emission is usually recurrent of interstitial oxygen. Emission to orange around 610 nm also results of interstitial oxygen defect [46]. As previously discussed, Ag also has the possibility of occupying two sites: substitutional Zn (Ag_{Zn}) and interstitial Zn (Ag_I). The Ag_{Zn} energy formation is known to be smaller than the one for Ag_I. Therefore, Ag uses to substitute Zn, moving the ZnO gap toward reduced energy levels and placing it as an excellent candidate for a p-type semiconductor [39]. In other words, the technique confirms the obtainment of ZnO and the partial substitution by Ag in its structure. Moreover, it also confirms the combined presence of Ag NPs.

Nanomaterials have been used as photocatalysts in degradative reactions since they have higher surface/volume ratio and, consequently, high specific area, improving the absorption of photons responsible for electron excitation. Another advantage associated to the use of nanomaterials in photocatalysis resides in the remarkable reduction of the probability of recombination of electron–hole pairs (transfer of the excited electron to its original state), due to the raise of the energy gap [48] verified with the reduction of the particle size. In particular, the highest indirect Tauc gap, 3.22 eV as shown in Fig. 4, is found for the ZnO10min-1 sample. It is thus possible to corroborate the photoluminescence spectrum, and the reduction of the density or absence of defects per oxygen vacancy, which also increases the photocatalytic efficiency (emission band with red shift).

3.2.2 *Magnetic properties*

The evaluation of the magnetic properties of the samples is performed through the analysis of the magnetization curves at specific temperatures and the dependence of magnetization under the FC and ZFC conditions.

Figure 9 shows the FC magnetization curves as a function of temperature for selected ZnO:Ag samples. The curves for the ZnO10min-0 and ZnO30min-0 show the expected behavior, with *M* of the order of memu/g and with a slight dependence with temperature. This fact may also be related to the presence of defects identified by the PL results (Fig. 8) and to the absence of Ag in these samples. Similar behavior has been already reported by different groups [24, 49], in which the authors discard the magnetic impurities as the origin of the magnetic properties of ZnO NPs.

Figure 10 presents the magnetization curves at specific temperatures for selected ZnO:Ag samples. The curves exhibit diamagnetic fingerprints verified for bulk ZnO material. However, a ferromagnetic-like contribution can be observed. This feature can be clearly evidenced after subtracting the diamagnetic background, not shown here. By "ferromagnetic-like" behavior we mean that the magnetization curves of these samples show most of the typical features of ferromagnetic materials, such as remanence, coercivity, and saturation.

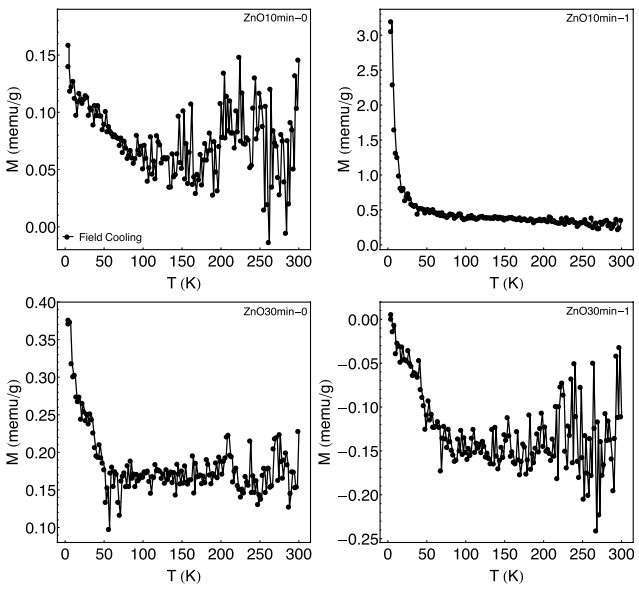

Fig. 9 Field-cooled magnetization curves as a function of temperature for selected ZnO:Ag samples. In particular, a static magnetic field of 200 Oe is applied in the sample during the process

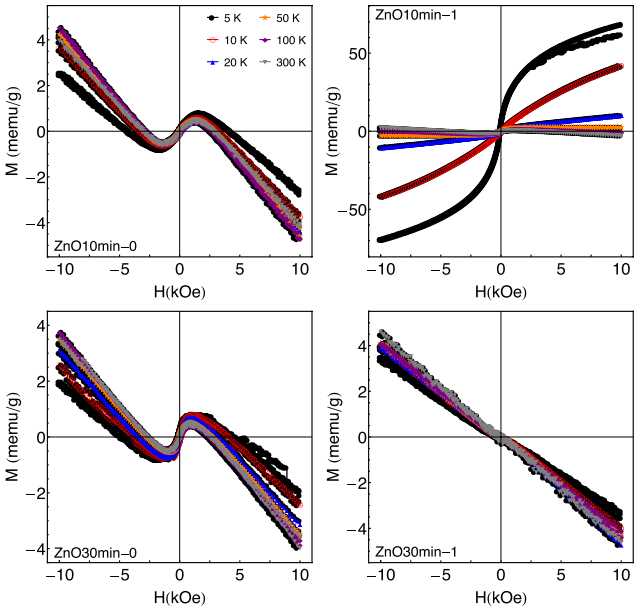

Fig. 10 Magnetization curves as a function of the field at specific temperatures for selected ZnO:Ag samples

The ZnO10min-0 and ZnO30min-0 samples present very similar magnetic behavior. On the other hand, for the samples with Ag, the behavior is quite different. The ZnO10min-1 sample reveals clear signs of ferromagnetism, remarkable increase of the magnetization, and strong dependence of *M* with the temperature. The ZnO30min-1 sample presents considerable reduction of the magnetization, although it still maintains ferromagnetic behavior. The presence of narrow hysteretic cycles is also verified. Similar results related to the magnetic behavior of ZnO:Ag samples have been previously reported by Gim et al. [24] and Garcia et al. [49].

The origin of ferromagnetism in ZnO and ZnO:Ag NPs is an interesting question and the complete comprehension of its origin is still lacking. In particular, one can attribute the magnetic behavior to several factors, such as nanosizing, defects, interface, substitution/doping, as well as a result of similar effects, e.g. expansion of the network/contraction, change in the electronic configuration, and quantum confinement [24].

The coexistence of Ag in the configuration of the NPs and as a dopant, verified through the XRD and PL techniques, also may lead to an interesting magnetism. It has already been reported that the coating of ZnO NPs by polymer molecules, a situation that is confirmed by transmission electron microscopy (Fig. 3), can lead to ferromagnetism at room temperature.

The magnetic properties of the pure ZnO and ZnO doped with Ag are in concordance with the expected effects for the produced NPs, confirmed by XRD and TEM, when compared to ZnO bulk. The NPs also show a slight increase in the structure of ZnO:Ag with respect to the pure ZnO, but still smaller lattice parameter values when compared to the bulk. In fact, it has recently been discovered that a change in the electronic structure of Au NPs and in the coating made up of organic molecules also lead to the appearance of the ferromagnetism, despite the diamagnetic character of the Au [50]. It can be related to a transfer of charge from the Au to the other element on the surface, giving rise to holes in the initially filled 5d orbital, due to a magnetic moment [51]. Similar arguments may be employed here in the case of Ag, which is typically diamagnetic.

According to our photoluminescence results, the polymer molecules present on the surface may control the number of combinations or induce new surface states that provide non-radiative decay paths, which is evidenced through the decrease of the emission intensity of the PL (contact quenching) (Fig. 8), showing ferromagnetic behavior [24], as well as hybridization. Alternatively, the low intensity bands by contact quenching and by doping/substitution can be correlated with the stronger magnetic behavior.

4 Conclusion

In conclusion, we have presented here a chemical route to synthesize stabilized ZnO:Ag NPs with nanosized metallic Ag using microwave-assisted hydrothermal synthesis. Moreover, we have investigated the structural, morphological, photocatalytic and magnetic properties of ZnO:Ag samples with different Ag concentrations, by employing XRD, field emission gun scanning electron microscopy, transmission electron microscopy, spectrophotometry, photodegradation, photoluminescence, and magnetic characterizations. In particular, we have focused on the obtainment of materials with good photocatalytic activity, low-intensity photoluminescence in the blue–orange region of the electromagnetic spectrum, and interesting magnetic properties.

The XRD results have indicated the standard wurtzite crystalline phases and face-centered cubic structure for the metallic Ag NPs. Through spectrophotometry, we have verified very good photocatalysis, in average time of 2 h and 30 min, of ZnO doped with 1 mol% silver synthesized at 10 min. All obtained powders have shown photoluminescence properties arisen from structural defects.

The partial substitution by Ag clusters has induced in the pure material a shift from green to yellow-red, which are lower energy wavelengths, and peak around 390 nm, related to the metal Ag NPs. Thus, these features have confirmed changes of the electrical properties due to the decreased gap. The magnetic properties have been interpreted in terms of nanosizing and similar effects. Under

these conditions, the partial substitution has improved the photocatalytics and magnetic properties of ZnO nanorods.

From a technological point of view, the production of reactors without the use of UV light lamps and with materials transparent to solar radiation may allow the application of heterogeneous photocatalysis in the degradation of polluting compounds or dirt. Post-treatment process is a serious disadvantage of ZnO. Post-treatment process is difficult and costly. To overcome this problem, magnetically separable compounds have been widely used in most industrial processes [22].

Such NPs may also be explored for biomedical applications and spintronic devices, given that they present interesting optical and magnetic properties. In this sense, our results make this material commercially viable, due to the reduced need of operational energy to photodegradation of microorganisms, pollutants, soils, among others. Moreover, our findings place the chemical route using microwave energy as a promising tool to produce stabilized NPs without any post-synthesis treatment.

Acknowledgements The research is supported by the Brazilian agencies CNPq, CAPES, and FAPERN.

References

1. L. Zhou et al., Chem. Eng. Res. Des. **98**, 36 (2015)
2. S. Mortazavi-Derazkola, S. Zinatloo-Ajabshir, M. Salavati-Niasari, Adv. Powder Technol. **28**, 747 (2017)
3. P. Bazant, I. Kuritka, M. Machovsky, T. Sedlacek, M. Pastorek, Mathematical Methods and Techniques in Engineering and Environmental Science, 341 (2011)
4. D.P. Volanti et al., Met e Mater. **63**, 352 (2007)
5. S. Rujitanapanich, P. Kumpapan, P. Wanjanoi, Energy Procedia **56**, 112 (2014)
6. M.A. Malik, M.Y. Wani, M.A. Hashim, Arab. J. Chem. **5**, 397 (2012)
7. M. Mozaffari, Z. Abooalizadeh, J. Amighian, J. Magn. Magn. Mater. **323**, 2997 (2011)
8. T.N. Ravishankar, T. Ramakrishnappa, G. Nagaraju, H. Rajanaika, Chem. Open **4**, 146 (2015)
9. D. Fu, P.G. Keech, X. Sun, J.C. Wren, Phys. Chem. Chem. Phys. **13**, 18523 (2011)
10. H.-Y. Li, F. Zhang, Preparation of nanoparticles by spray-drying and their use for efficient pulmonary drug delivery. Nanoparticles Biol. Med. **906**, 295–301 (2012)
11. T. Zaki, K.I. Kabel, H. Hassan, Ceram. Int. **38**, 4861 (2012)
12. R.F. Khairutdinov, Russ. Chem. Rev. **67**, 109 (1998)
13. J. Villaseñor, P. Reyes, G. Pecchi, J. Chem. Technol. Biotechnol. **72**, 105 (1998)
14. A. Music, J. Batista, J. Levec, Appl. Catal. A **165**, 115 (1997)
15. D. Zhang, T. Yang, Q. Wang, D. Zhang, Mater. Chem. Phys. **68**, 233 (2001)
16. D. Look, C. Cokun, B. Claflin, G. Farlow, Phys. B **340–342**, 32 (2003)
17. M. Purica, E. Budianu, E. Rusu, Microelectron. Eng. **51–52**, 425 (2000)
18. C.-C. Lin, H.-P. Chen, S.-Y. Chen, Chem. Phys. Lett. **404**, 30 (2005)
19. M. Schubnell, I. Kamber, P. Beaud, Appl. Phys. A **64**, 109 (1996)
20. B. Tryba, M. Piszcz, A. Morawski, Open Mater. Sci. J. **4**, 5 (2010)
21. Y. Zheng et al., J. Phys. Chem. C **112**, 10773 (2008)
22. S. Mortazavi-Derazkola, M. Salavati-Niasari, O. Amiri, A. Abbasi, J. Energy Chem. **26**, 17 (2017)
23. S. Hosseini, I.A. Sarsari, P. Kameli, H. Salamati, J. Alloys Compd. **640**, 408 (2015)
24. J.S. Gim et al., Appl. Phys. Express **6**, 063005 (2013)
25. X. Wang et al., RSC Adv. **5**, 8622 (2015)
26. V.D. Araújo et al., CrystEngComm **14**, 1150 (2012)
27. M. Taguchi et al., CrystEngComm **14**, 2117 (2012)
28. G. Qiu et al., J. Phys. Chem. C **116**, 468 (2012)
29. S.-B. Kim, Met. Mater. Int. **8**, 455 (2002)
30. A.B. Panda, G. Glaspell, M.S. El-Shall, J. Phys. Chem. C **111**, 1861 (2007)
31. W. Si, J.Y. Yu, Q. Li, Adv. Mater. Res. **299–300**, 542 (2011)
32. S.Q. Chen, Y. Wang, J. Mater. Chem. **20**, 9735 (2010)
33. C. Parada, E. Morán, Chem. Mater. **18**, 2719 (2006)
34. N.L. Pacioni, C.D. Borsarelli, V. Rey, A.V. Veglia, *Synthetic routes for the preparation of silver nanoparticles* (Springer, Berlin, 2015), pp. 13–46
35. T.T. Ha, T.D. Canh, N.V. Tuyen, ISRN Nanotechnol. **2013**, 1 (2013)
36. N. Yusoff, L.-N. Ho, S.-A. Ong, Y.-S. Wong, W. Khalik, Desalin. Water Treat. **57**, 12496 (2016)
37. A.S. Edelstein, R.C. Cammaratra, *Nanomaterials: synthesis, properties and applications* (CRC Press, Boca Raton, 1998)
38. M. Zawadzki, Solid State Sci. **8**, 14 (2006)
39. V. Khranovskyy, I. Tsiaoussis, M. Eriksson, R. Yakimova, Phys. Status Solidi **211**, 2109 (2014)
40. V. Uskoković, Rev. Chem. Eng. **23**, 301 (2007)
41. A.S. Kuznetsov et al., Opt. Mater. Express **2**, 723 (2012)
42. A.J.C. Lanfredi, R.R. Geraldes, O.M. Berengue, E.R. Leite, A.J. Chiquito, J. Appl. Phys. **105**, 023708 (2009)
43. U. Woggon, *Optical properties of semicondutor quantum dots* (Springer, Berlin, 1996)
44. J.B. Galvez et al., *Purificación de águas por fotocatálisis heterogénea: estado del arte* (Digital Graf., La Plata, 2001)
45. J. Al-Sabahi, T. Bora, M. Al-Abri, J. Dutta, Materials **9**, 238 (2016)
46. F. Han et al., Opt. Express **22**, 11436 (2014)
47. S. Kuriakose, V. Choudhary, B. Satpati, S. Mohapatra, Beilstein J. Nanotechnol. **5**, 639 (2014)
48. J. Li, Y. Xu, Y. Liu, D. Wu, Y. Sun, China Particuology **2**, 266 (2004)
49. M.A. Garcia et al., Nano Lett. **7**, 1489 (2007)
50. A. Hernando et al., Phys. Rev. B **74**, 052403 (2006)
51. P. Zhang, T.K. Sham, Phys. Rev. Lett. **90**, 245502 (2003)